

Article

Study on the Effects of Different Water Content Rates on the Strength and Brittle Plasticity of Limestone

Quan Zhang ¹, Yuanming Liu ^{1,*}, Guohua He ², Qingzhi Chen ¹, Xun Ou ¹  and Jiao Tian ³¹ College of Civil Engineering, Guizhou University, Guiyang 550025, China² Guizhou Expressway Group Co., Ltd., Guiyang 550004, China³ Guizhou Transportation Planning Survey & Design Academe Co., Ltd., Guiyang 550001, China

* Correspondence: liuym_2021@163.com; Tel.: +86-136-485-063-68

Abstract: Water can deteriorate the compositional properties of rock through softening and dissolution. The water content rate of rock has a certain effect and can cause changes in rock properties caused by the water action. In this research, to study the effects of the water content rate on the strength and brittle plasticity of limestone, uniaxial compression tests with different water content rate states were conducted, and the form of limestone damage under different water content rate conditions was analyzed. The effects of the different water content rates on the modulus of elasticity, uniaxial compressive strength, brittleness index B value, and brittleness correction index BIM value (BIM: the ratio of dissipated strain energy to releasable elastic strain energy at the peak point of the specimen) of limestone were investigated. It was found that as the rate of water content in the limestone increased from 0% to 0.27%, the penetration shear surface on the limestone's damaged surface decreased. The modulus of elasticity decreased from 8.85 to 6.76 GPa, the uniaxial compressive strength decreased from 74.11 to 57.60 MPa, the brittleness index B value decreased from 1.17 to 1.04, and the brittleness correction index BIM value increased from 0.09 to 0.26. As the rate of water content on the limestone increased, the rock's modulus of elasticity and uniaxial compressive strength decreased. Additionally, the rock's brittleness decreased, and the percentage of plastic deformation in the total deformation increased.

Keywords: softening of limestone; uniaxial compression test; forms of destruction; intensity value; brittle value; brittleness correction value; different water content rates



Citation: Zhang, Q.; Liu, Y.; He, G.; Chen, Q.; Ou, X.; Tian, J. Study on the Effects of Different Water Content Rates on the Strength and Brittle Plasticity of Limestone. *Appl. Sci.* **2023**, *13*, 4685. <https://doi.org/10.3390/app13084685>

Academic Editor: Giuseppe Lazzara

Received: 19 February 2023

Revised: 28 March 2023

Accepted: 30 March 2023

Published: 7 April 2023



Copyright: © 2023 by the authors. Licensee MDPI, Basel, Switzerland. This article is an open access article distributed under the terms and conditions of the Creative Commons Attribution (CC BY) license (<https://creativecommons.org/licenses/by/4.0/>).

1. Introduction

Rocks are a collection of various minerals in nature and contain various fractures and pores [1–4]. When rocks are soaked in water, the water penetrates into the rock through these fractures and chemically and physically interacts with the minerals inside the rock to deteriorate the properties of the rock [5–7]. The mechanical properties of the rock mass under the interaction of water and rock must be different from the properties of the rock mass in a natural air-drying state [8–10]. During an actual tunnel excavation, the abundant joints, layers, and fractures in the surrounding rock can cause groundwater to leak in or infiltrate, which will affect the overall strength and failure characteristics of the surrounding rock [11–14]. In slope engineering, foundation pit excavation, chamber excavation, and other practical engineering projects, it was demonstrated that if the chamber is subjected to a long-term immersion in water, the chamber and slope can collapse and become damaged, threatening construction safety. The interaction between water and rock has attracted the attention of many experts and scholars. Many scholars have studied the mechanical properties of rocks with different moisture contents.

For example, CAI Xin [15] conducted dynamic Brazilian disk experiments on Yunnan sandstone samples with different water contents. The test results showed that for each water content level, the dynamic tensile strength of sandstone is positively sensitive to

the loading rate. Lin Hanxiang [16] conducted Triaxial compression rheological tests on argillaceous siltstone with different water contents and studied the effects of both the water content and stress levels on creep strain, creep rate, long-term strength, and creep failure mode. The test results show that the time-dependent characteristics of rock are gradually activated as the water content and stress levels increase. The water content and stress levels greatly increase the instantaneous strain, creep strain, and the steady creep strain rate. Zhao Kui [17] carried out uniaxial compression tests on red sandstone with different water contents; the results indicate that the peak strength of red sandstone in both natural and saturated states is 26.13% and 41.75% lower than that of red sandstone in a dry state. By increasing the water content, the dominant failure pattern of the rock specimens changes from tension failure to shear failure. Huang Xin [18] conducted uniaxial compression tests and Engineering Discrete Element Method (EDEM) numerical simulation tests on sandstone with different water contents to study the influence of different water contents on the mechanical properties of sandstone. The findings demonstrated that as the water content in the sample's grew, the peak strain increased but the peak strength, elastic modulus, maximum energy rate of the individual acoustic emission events, and cumulative acoustic emission energy rates all reduced. Zhen Wei [19] used the split Hopkinson pressure bar test system to test disc coal samples with different water contents. The results demonstrated that the dynamic stress–strain curve of the coal samples consisted of four stages. As the water content increased, the brittleness of the coal samples decreased and ductility was enhanced. Qin Xinzhan [20] conducted a uniaxial compression test on sandstone samples with different water contents and an acoustic emission (AE) analysis. The test results show that by increasing the water content rate, the uniaxial compressive strength of sandstone decreases following a negative exponential relationship. There was some similarity between the AE signals of the sandstone samples with the different water content rates. Li Chuanming [21] carried out a uniaxial compression test and a Brazilian splitting test on white sandstone samples with different water contents. The experimental results showed that uniaxial compressive strength, tensile strength, and elastic modulus all decline as the moisture content increases. Zhu Jun [22] conducted a series of direct tensile tests on marble rocks with different water contents. The test results show that the tensile strength of the marble rock significantly decreases as the water content increases, characterizing variable fracture surfaces. Zhang Yaoyao [23] conducted triaxial tests on granite with free maximum moisture content and studied the deformation and failure characteristics and mechanisms of granite. Yu Yongjiang [24] carried out creep disturbance tests on mudstone specimens with different water content levels under fractional loading. The results show that an increase in the moisture content leads to a significant increase in the creep failure strain of mudstone and that the accelerated creep rate is greatly accelerated. Moreover, as the moisture content increases, the type of mudstone creep disturbance failure gradually changes from accelerated creep failure to disturbance failure. However, it should be noted that the above research is more aimed at the influence of the different moisture contents on the rock strength indicators. There remains a lack of research on the brittleness and plasticity of rocks under an aqueous environment. Therefore, it is necessary to study the strength and brittleness of rocks under different moisture content conditions.

Guizhou Province is a region with a wide distribution of karst landforms. Here, carbonate, sulfate, and halide saltstones are commonplace, and the nature of the rock masses is easily affected by groundwater and surface water. The area containing a tunnel under construction features a variety of lithological properties; complex combinations of weathered mudstone, argillaceous limestone, and limestone are widely distributed and jointed fractures in the rock mass are commonly found. Additionally, unfavorable geological conditions, such as folds and faults are very common, and the region is rich in atmospheric precipitation. Here, surface water directly infiltrates into the ground, and the main source of groundwater recharge is sufficient. In addition, during the tunnel excavation process, the original rock mass will inevitably become disturbed, thereby increasing the seepage path of the groundwater into the rock mass, resulting in a change in

moisture content in the surrounding rock of the tunnel. Therefore, it is of great practical and theoretical significance to clarify whether the interaction between the water and rock will lead to changes in the strength and failure characteristics of a rock mass under different moisture content conditions and whether these changes will threaten the safety of tunnel engineering.

Based on the previous studies, we select the widely distributed limestone in the surrounding rock of Tongzi Tunnel as the representative sample and use the uniaxial compression test method to study the mechanical properties, brittleness indexes, and plastic deformation of limestone with different moisture contents.

2. Specimen Preparation and Test Methods

2.1. Specimen Preparation

The limestone of the face of Tongzi Tunnel (YK42+395) was sampled according to the Highway Engineering Rock Test Regulations (JTG E41-2005) and cut and polished to form a cylindrical specimen with a diameter of 50 mm and a height of 100 mm. The specimen is shown in Figure 1.



Figure 1. Limestone specimens.

There are many factors affecting the uniaxial compression test results of limestone, but the main focus of this paper is studying the effects of the different water content rates on the uniaxial compression test results of limestone. Therefore, in the process of test sample selection, 10 cylindrical specimens were subjected to acoustic wave detection with an NM-4A non-metallic ultrasonic detection analyzer, and the specimens with similar wave speeds were selected for the subsequent experiments. The acoustic detection results are shown in Table 1. This process was performed to reduce the influence of the variability of the limestone samples themselves on the test results.

Table 1. Specimen acoustic test data.

Test Piece Number	E1	E2	E3	E4	E5	E6	E7	E8	E9	E10
Sonics peed Km/s	5.81	5.88	5.85	5.56	5.95	5.56	5.43	5.81	5.81	5.81

Based on the results of the wave velocity testing, four limestone specimens, E1, E8, E9, and E10 were selected for the uniaxial compression tests with different water content rates. The four specimens, E1, E8, E9, and E10 were inserted into a 202-2AB electric thermostatic oven for drying at 105 degrees for 24 h according to the Rock Test Procedure for Highway Engineering (JTG E41-2005). We then placed the dried specimens in the drying oven for natural cooling. After cooling, we weighed the specimens with an electronic scale with an accuracy of 0.01 g. The above dried specimens were soaked using the free immersion method, which means that the dried specimens were directly placed into the water to control the water content by controlling the immersion time to obtain specimens with different moisture contents, and the specimens were also weighed using the same quality measurement tool after the immersion was completed. The mass after drying, length of immersion, mass after immersion, and the final calculated results of the water content rates

of limestone obtained for each specimen are shown in Table 2. The formula for calculating the water content rate is as follows:

$$\lambda = \frac{M_1 - M_2}{M_2} \times \% \quad (1)$$

where λ is the rate of water content in the limestone (%), M_1 is the weight of the limestone specimen after immersion (g), and M_2 is the weight of the limestone specimen after drying (g).

Table 2. The dried mass, soaking duration, soaking mass, and moisture content of each sample.

Test Piece Number	E1	E8	E9	E10
M_2	477.76	478.88	479.29	478.65
Soaking time (d)	0	1	1.5	2
M_1	477.76	479.22	479.79	479.94
λ	0.00	0.07	0.10	0.27

2.2. Test Methods

For testing, we used an RMT-301 rock and concrete mechanical test system, which is a computer-controlled multi-functional electro-hydraulic servo-testing machine specially designed to analyze the mechanical properties of rock and concrete materials in line with the corresponding national standards. The system has the advantages of convenient operation, good control performance, a high degree of automation, high measurement and control accuracy, high rigidity, and good long-term stability. In this study, a uniaxial compression test was used to control the loading, and the change rate of the loading displacement was set to 0.005 mm/s in the test. The machine was loaded along the axial direction until the specimen was destroyed as shown in Figure 2.

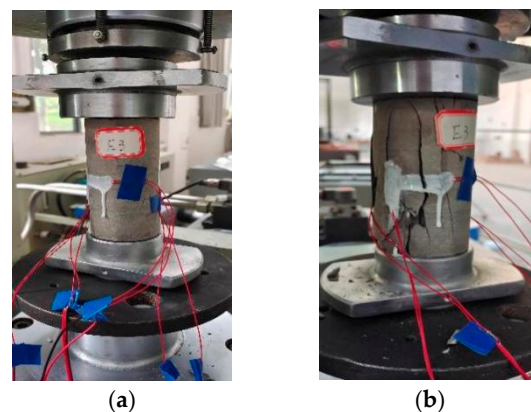


Figure 2. Experimental process. (a) Before the specimen experiment, (b) after the specimen experiment.

3. Uniaxial Compression Test Results Analysis

According to the data from the uniaxial compression test, the stress–strain curves of the limestone specimens with different water content rates were drawn as shown in Figure 3, where the X axis represents the axial strain amplified 100 times in the process of the uniaxial compression of the limestone specimen, and the Y axis represents the axial stress in the process of the uniaxial compression of the limestone specimen. As shown in Figure 3, the development trend of the stress–strain curves is similar between the limestone specimens with the different water content rates, which can be divided into five stages. First, the characteristics of each stage are analyzed as follows.

3.1. First Stage: The Fracture Compaction Stage (1)

Here, the stress–strain curve is concave. In this stage, when the axial strain of the limestone samples with the different water content rates reaches 0.3%, the stress of E1 is 13.45 MPa, that of E8 is 13.38 Mpa, that of E9 is 11.79 Mpa, and that of E10 is 10.82 MPa. With an increase in the rate of water in the limestone samples, the limestone samples achieve the same axial strain, and the corresponding axial stress is smaller. This phenomenon may be caused by an increase in the water content, causing the micro-cracks and micro-cavities in the limestone to fill with water. Therefore, when the limestone is compacted by an external force, the lower the water content, the greater the external force, and the greater the water content, the smaller the external force.

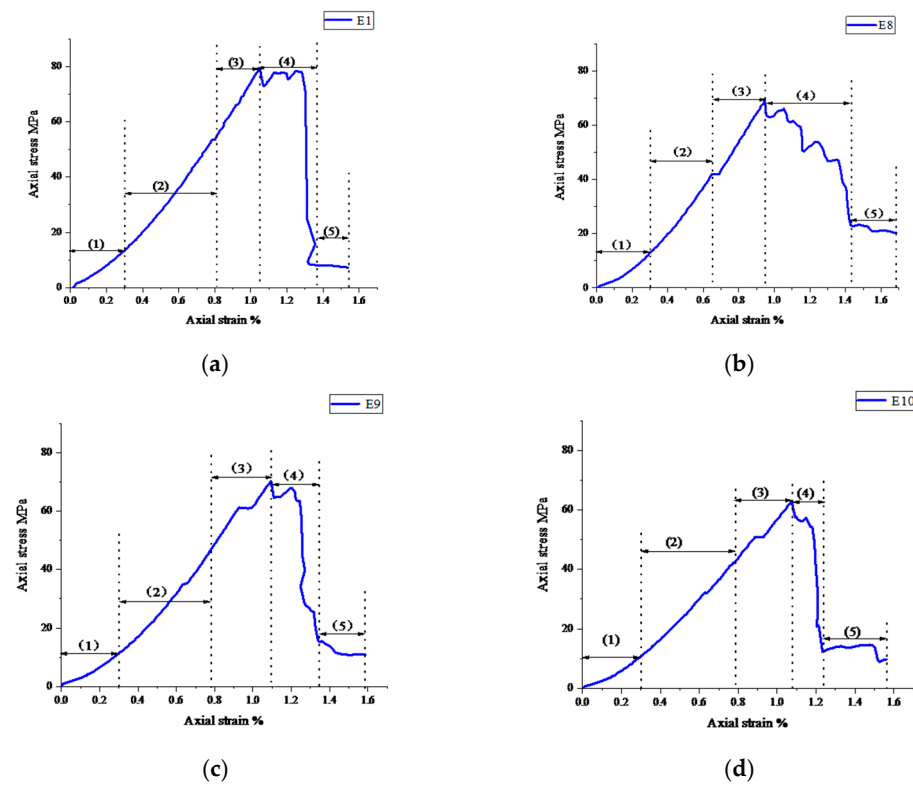


Figure 3. Stress–strain curve. (a) Test piece E1, (b) test piece E8, (c) test piece E9, (d) test piece E10.

3.2. Second Stage: Stable Development of Elastic Deformation to Microelastic Fractures (2)

At this stage, the stress–strain curve is approximately linear, and the stress and strain are proportional. Here, the ratio of the stress and strain is the elastic modulus of the rock. Therefore, the elastic moduli of the limestone specimens with the different water content rates can be obtained using the linear fitting function in Origin as shown in Table 3.

Table 3. Elastic modulus of limestone samples with different water content rates.

Test Piece Number	E1	E8	E9	E10
Elastic modulus (GPa)	8.85	8.65	7.82	6.76

The data in Table 3 were then plotted as shown in Figure 4. According to Table 3 and Figure 4, when the rate of the limestone water content is 0%, 0.07%, 0.10%, and 0.27%, the corresponding elastic moduli are 8.846, 8.651, 7.824, and 6.762 GPa, respectively. It can be seen that the elastic modulus of the limestone decreases with an increase in the rate of the water content in the limestone.

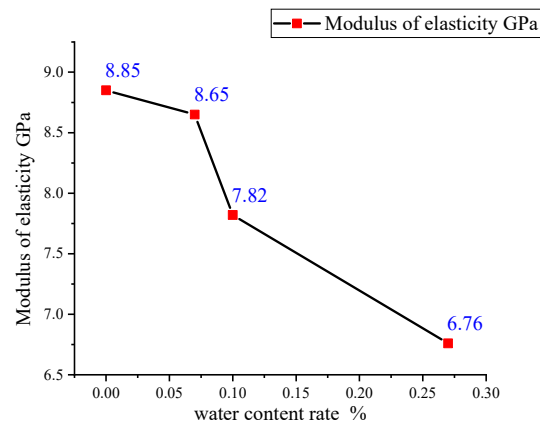


Figure 4. Modulus elasticity of limestone samples with different water content rates.

3.3. Third Stage: The Progressive Rupture Stage (3)

At this stage, the microfractures in the rock continue to develop until they fail. The corresponding stress at the time of failure is the peak point of the stress–strain curve, and the uniaxial compressive strength of the test piece. The uniaxial compressive strength of the rock is shown in Table 4. We then plotted the data presented in Table 4 as shown in Figure 5.

Table 4. Uniaxial compressive strength of limestone specimens with different water content rates.

Test Piece Number	E1	E8	E9	E10
Uniaxial compression Strength MPa	74.11	64.73	63.70	57.60

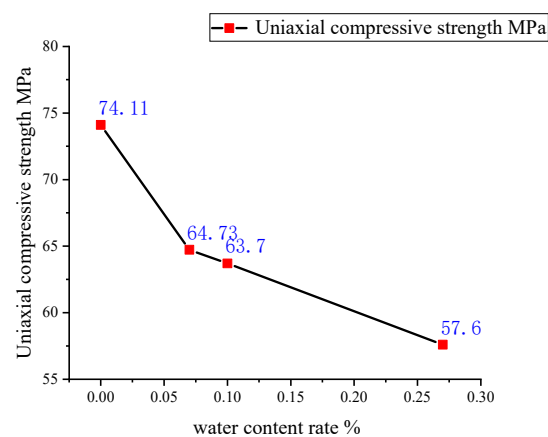


Figure 5. Uniaxial compressive strength of limestone samples with different water content rates.

According to Table 4 and Figure 5, when the rate of the limestone water content is 0%, 0.07%, 0.10%, and 0.27% the corresponding uniaxial compressive strength is 74.109, 764.727, 63.699, and 57.6 MPa. It can be seen that the uniaxial compressive strength of the limestone decreases gradually with an increase in the percentage of the water content in the limestone samples.

3.4. Fourth Stage: The Post-Rupture Stage (4)

At this stage, the stress–strain curve is bimodal in shape. After the stress reaches its peak, the stress first decreases and then increases as the strain increases. As the water content rate increases, the top of the second peak gradually decreases. The main reason for this phenomenon is that the increase in water content causes the rock to change from

brittle to plastic. The uniaxial compressive strength of the test piece can also be obtained. At this stage, the stress decreases sharply as the strain increases.

3.5. Fifth Stage: The Residual Stress Stage (5)

At this stage, the test pieces with a moisture content of 0 present the lowest residual stress. Rocks that do not contain water are brittle, and when the rock is broken, the internal structure of the rock is basically destroyed. Thus, the residual stress is very low. The residual stress of the different moisture content specimens is higher than that of the non-water specimens because water will make the rock change from brittle to plastic.

4. Prototype Analysis of Specimen Failure

The form of uniaxial compression failure in the limestone specimens with the different water content rates is shown in Figure 6. It can be seen from Figure 6 that when the water content rate of the limestone samples is 0%, 0.07%, 0.1%, and 0.27% there are more splitting surfaces along the axial direction of the failure surface of the sample with one or more shear failure surfaces running through the entire rock sample. Here, the shear failure surface caused by the low tensile strength of the rock is the main cause of the specimen failure.

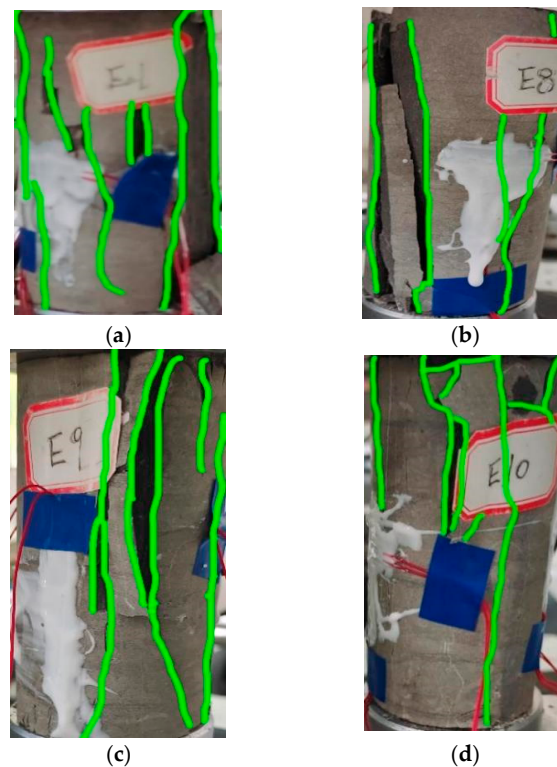


Figure 6. Failure diagram of limestone samples with different water content rates. (a) Water content rate 0%, (b) water content rate 0.07%, (c) water content rate 0.1%, (d) water content rate 0.27%.

The failure forms of the limestone samples with the different water content rates were then analyzed. We found that when the water content rate of the limestone sample is 0% and 0.07%, the sample presents an obvious caving phenomenon in the failure process, that is, one side of the specimen peels off directly along the failure surface due to its high brittleness. When the water content rate of the limestone sample is 0.1%, a phenomenon similar to “pressure rod instability” is observable in the test piece (i.e., the shear slip surface appears inside the rock sample, and the axial tension split surface caused by the slip surface causes the material of the rock sample to detach from the main body and become a pressure rod, which is broken due to instability [25]). When the water content rate of the limestone sample is 0.27%, the failure cracks appear primarily in the upper part of the test piece, except for one crack that runs through the entire test piece.

Based on the above analysis, conclusions can be drawn as follows: With an increase in the water content rate, the decrease in the penetration failure surface of the limestone sample may be caused by an increase in the water content rate; with an increase in the water content rate, the specimen develops from brittle failure to plastic failure.

To verify this conjecture, we next calculate the brittleness index of the above limestone samples quantitatively and represent the brittleness degree of each sample in the form of data. Many scholars at home and abroad have studied the brittleness of rock and have given the corresponding formulae for calculating the brittleness index.

B. Tarasov and Y. Potvin [26] proposed a method to calculate the brittleness index based on the fracture angle during rock failure. R. Rickman [27] proposed a brittleness index calculation method based on the normalized elastic modulus and Poisson’s ratio of rocks. R. Altindag [28] proposed a brittleness index calculation method based on calculating the peak value and residual strength of rocks. Liao Dongliang [29] proposed a calculation method for the brittleness index based on the mineral composition and fracture toughness of rock.

This paper is based on the stress–strain curve obtained from a uniaxial compression test. Based on the method of Cao Yangbing and Zhou Hui [30,31], et al., the brittleness index of the above limestone samples was quantitatively calculated, and the brittleness degree of the failure of each limestone sample was represented as data using the following calculation formula:

$$B = B_{d1} + B_{d2} \tag{2}$$

$$B_{d1} = \frac{\lg(\frac{1}{\epsilon_p})}{K} \tag{3}$$

$$B_{d2} = \frac{(\sigma_p - \sigma_r)}{\sigma_p t} + \frac{(\epsilon_r - \epsilon_p)}{\epsilon_p t} \tag{4}$$

where B is the rock brittleness indicator, B_{d1} is the indicator of brittleness before rock peaks, B_{d2} represents the indicators of brittleness after rock peaks, σ_p is the uniaxial compressive strength of the rock, σ_r is the residual strength of the rock, ϵ_p is the corresponding strain when the stress reaches its peak, ϵ_r is the strain corresponding to the residual strength of the rock, t is the time interval between the peak strength point on the stress–strain curve and the starting point of the residual strength, and K is a constant ($K = 5$).

The parameters of the limestone samples with different water content rates are shown in Table 5.

Table 5. Parameters required for calculating the brittleness index of limestone samples with different water content rates.

Test Piece Number	σ_p (MPa)	ϵ_p (%)	σ_r (MPa)	ϵ_r (%)	t (s)
E1	74.11	1.04	7.86	1.38	1.5
E8	64.73	0.94	21.02	1.42	1.7
E9	63.70	1.08	17.23	1.36	1.4
E10	57.60	1.09	15.39	1.23	1.3

The brittleness index B values of the calculated limestone are shown in Table 6.

Table 6. Graystone brittleness index values.

Test Piece Number	E1	E8	E9	E10
B_{d1}	0.40	0.50	0.39	0.39
B_{d2}	0.77	0.64	0.67	0.65
B	1.17	1.14	1.06	1.04

The calculation results of the brittleness index B value were plotted as shown in Figure 7.

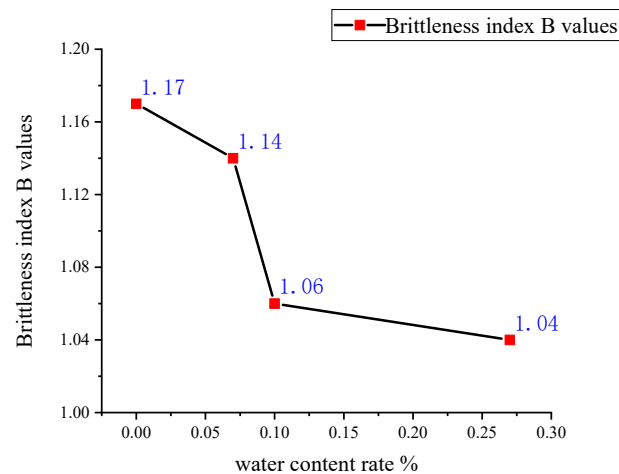


Figure 7. Brittleness index B values of limestone samples with different water content rates.

According to the results presented in Table 6 and Figure 7, when the water content rate of the limestone is 0%, 0.07%, 0.10%, and 0.27%, the brittleness index B values are 1.165, 1.142, 1.060, and 1.044, respectively.

The above analysis shows that with an increase in the limestone water content rate, the brittleness index of the limestone shows a downward trend. This result also verifies the conjecture that the brittleness of the limestone decreases gradually with an increase in the limestone water content rate.

Whether or not the plastic deformation of the limestone increases with an increase in the limestone water content rate will be discussed in the energy analysis section.

5. Analysis of Energy and Brittleness of Plasticity under Uniaxial Compression

M. Aubertin defines the ratio (U^d/U^e) of the dissipated strain energy to the releasable elastic strain energy at the peak point of the specimen as the brittleness index correction value (BIM). The larger the BIM value is, the smaller the ratio of the pre-peak elastic deformation to the total pre-peak deformation becomes, indicating a greater plastic deformation [32,33]. Therefore, to determine whether the proportion of plastic deformation among the total deformation in the limestone samples increases with an increase in the moisture content, it is necessary to analyze the energy evolution characteristics of the limestone samples with different water content rates in a uniaxial process.

Assuming that the specimen does not engage in heat exchange with the outside world during the uniaxial compression test, the specimen is considered a closed system.

The total input strain energy generated by the work performed by the external force is U , which uses the following formula according to the first law of thermodynamics [34]:

$$U = U^d + U^e \quad (5)$$

where U is the total strain energy of the external force work input (KJ/m^3), U^d is the dissipative energy (KJ/m^3), and U^e is the elastic strain energy that can be released (KJ/m^3).

The relationship between the dissipative energy U^d and the releasable elastic strain energy U^e is shown in Figure 8.

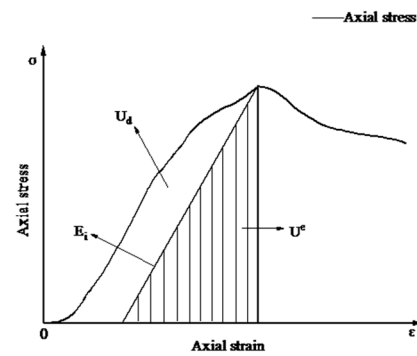


Figure 8. The energy relationship between U^d and U^e per unit volume of rock.

In Figure 8, the stress–strain curve and the unloading elastic modulus E_i are enclosed by U^d , and the shaded part U^e represents the release of elastic strain energy.

The expression of each instance of strain energy during the uniaxial compression test is as follows:

$$U = \int_0^{\varepsilon_1} \sigma_1 d\varepsilon_1 \tag{6}$$

$$U^e = \frac{\sigma_1^2}{2E_0} \tag{7}$$

$$U^d = \int_0^{\varepsilon_1} \sigma_1 d\varepsilon_1 - \frac{\sigma_1^2}{2E_0} \tag{8}$$

where σ_1 is the main stress, E_0 is the initial elastic modulus of the specimen, and ε_1 is the strain in the direction of the main stress.

Using Equations (6)–(8), the total strain energy U , dissipative energy U^d , and releasable elastic strain energy U^e corresponding to the peak points of the different water content rates can be obtained as shown in Table 7. The ratio of the releasable elastic strain energy and the dissipative energy to the total input strain energy of each test piece is then plotted as shown in Figure 9.

As shown in Table 7, most of the total input strain energy of the different water content rate specimens in the uniaxial compression process is stored as releasable strain energy, and the rest is dissipated by rock damage and plastic deformation. As can be seen from Figure 9, the ratio of the releasable elastic strain energy to the total input strain energy gradually decreases with an increase in water content rate, while the ratio of dissipative energy gradually increases. The energy dissipation will induce the deterioration of the specimen and reduce its strength. Therefore, as the water content rate of the test piece increases, the strength of the test piece decreases.

Most of the total strain energy input in the uniaxial compression process of limestone is stored as elastic strain energy that can be released. When the input energy is greater than the elastic energy storage limit of the rock itself, the rock begins to fracture and become unstable and releases energy to the outside world. From the calculation results of Table 7, it can be seen that with an increase in the moisture content, the elastic storage energy limit of the limestone gradually decreases. The elastic strain energy storage of a rock depends on the voids and microfractures inside the rock. The storage principle of rock strain energy is that the energy input from the outside is stored through the closure of voids and microfractures. When the moisture content increases, the voids and microfractures inside the rock are filled by moisture, decreasing the upper limit of energy that the rock can store.

Table 7. The strain energy corresponding to the peak point of each specimen.

Specimen Number	Total Input Strain Energy U	Releases Elasticity Strain Energy U^e	Dissipative Energy U^d
E1	338.15	310.43	27.72
E8	263.49	242.15	21.24
E9	303.16	259.30	43.86
E10	313.45	245.32	68.13

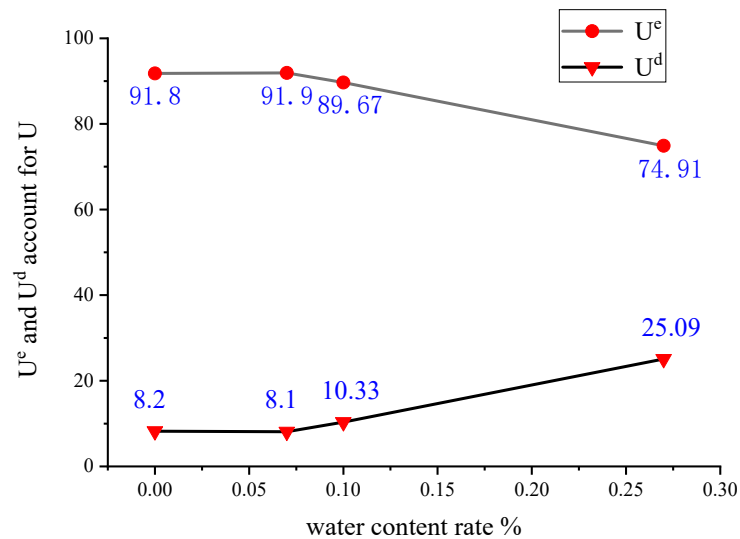


Figure 9. U^e and U^d account for U.

The ratio (U^d/U^e) of the dissipated strain energy to the releasable elastic strain energy at the peak point of the specimen is defined as the brittleness index correction value (BIM). The BIM values of each specimen were calculated as shown in Table 8.

Table 8. The BIM value of each test piece.

Specimen Number	E1	E8	E9	E10
BIM value	0.09	0.09	0.17	0.28

The BIM values in Table 8 are plotted in Figure 10.

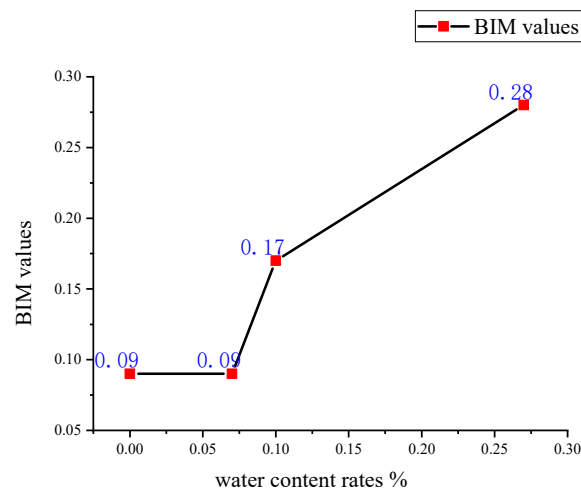


Figure 10. BIM values of limestones with different water content rates.

It can be seen from Table 8 and Figure 10 that when the water content rate of limestone is 0%, 0.07%, 0.10%, and 0.27%, the brittle index correction values (BIMs) are 0.089, 0.088, 0.179, and 0.263, respectively.

From the above analysis, it can be seen that with an increase in the water content rate, the overall development trend for the BIM of the limestone samples increases, i.e., the proportion of plastic deformation in the total deformation increases. This result also validates the conjecture proposed earlier that with an increase in the water content rate of the limestone sample, the brittleness of the rock sample gradually decreases, and the plasticity gradually increases.

6. Conclusions

Based on the indoor test and the theoretical analysis of the tunnel limestone, the following conclusions can be drawn:

1. With an increase in the limestone water content rate, the pores and micro-cracks inside the limestone are filled with water, which increases the stress required in the compaction stage of the limestone. At the same time, with an increase in the water content rate of the limestone, the elastic modulus and uniaxial compressive strength of the limestone gradually decrease.
2. With an increase in the water content rate of the limestone, the failure form is still mainly tensile failure. However, after an increase in the water content rate, the through-surface of the specimen failure gradually decreases. Then, based on the quantitative calculations, the brittleness index of the limestone will decrease with an increase in the water content rate.
3. With an increase in the limestone water content rate, the upper limit of the elastic strain energy storage will decrease because the pores and micro-cracks inside the limestone become filled with water. In addition, the dissipation energy of limestone will increase with an increase in the water content rate, thereby reducing the strength of the limestone. The proportion of pre-peak deformation among the total deformation increases with an increase in the water content rate of the limestone, i.e., the molding of the limestone increases.
4. This paper mainly studied the effects of the water content rate on the mechanical properties of limestone, which has certain limitations. The test results were also affected by the sample size. However, the final test results showed good regularity with a high reliability. Thus, this study could provide a reference for research on other kinds of rock hydrologic properties. In addition, since this research considered Tongzi Tunnel as its research background (based on the actual project), this work has very important practical significance. The results could provide theoretical support and guidance for the excavation of Tongzi tunnel, including the stability of the surrounding rock and maintenance during subsequent periods.

Author Contributions: Conceptualization, Q.Z.; methodology, Q.Z. and Y.L.; software, Q.Z. and Q.C.; validation: Q.Z., G.H. and Y.L.; investigation, Q.Z. and Y.L.; resources, Y.L.; writing-review and editing; Q.Z. and X.O.; visualization, Q.Z., J.T. and Q.C.; supervision, Y.L., G.H., X.O., Q.C. and J.T. All authors have read and agreed to the published version of the manuscript.

Funding: This work is supported by the Yuanming Liu: Major Science and Technology Special Project of Guizhou Province (Qiankehe Major Special Project [2018] 3011); the Natural Science Foundation of Guizhou Province (Qiankehe Foundation-ZK [2022] General 082); Research on Key Technology of Guiyang Urban Rail Transit Tunnel Underpass Existing Railway (2020-13-ZB); and the Natural Science Foundation of Guizhou Province (Qiankehe Foundation [2019] No. 1057).

Informed Consent Statement: Not applicable.

Data Availability Statement: Data sharing is not applicable.

Conflicts of Interest: The authors declare no conflict of interest.

References

1. Meng, F.; Wong, L.N.Y.; Zhou, H. Rock brittleness indices and their applications to different fields of rock engineering: A review. *J. Rock Mech. Geotech. Eng.* **2021**, *13*, 221–247. [[CrossRef](#)]
2. Yang, C.; Liu, J. Petroleum rock mechanics: An area worthy of focus in geo-energy research. *Adv. Geo Energy Res.* **2021**, *5*, 351–352. [[CrossRef](#)]
3. Li, X.; Wei, W.; Wang, L.; Ding, P.; Zhu, L.; Cai, J. A new method for evaluating the pore structure complexity of digital rocks based on the relative value of fractal dimension. *Mar. Pet. Geol.* **2022**, *141*, 105694. [[CrossRef](#)]
4. Askaripour, M.; Saeidi, A.; Mercier-Langevin, P.; Rouleau, A. A review of relationship between texture characteristic and mechanical properties of rock. *Geotechnics* **2022**, *2*, 262–296. [[CrossRef](#)]
5. Torres-Suarez, M.C.; Alarcon-Guzman, A.; Moya, R.B.-D. Effects of loading–unloading and wetting–drying cycles on geomechanical behaviors of mudrocks in the Colombian Andes. *J. Rock Mech. Geotech. Eng.* **2014**, *6*, 257–268. [[CrossRef](#)]
6. Roy, D.G.; Singh, T.N.; Kodikara, J.; Das, R. Effect of water saturation on the fracture and mechanical properties of sedimentary rocks. *Rock Mech. Rock Eng.* **2017**, *50*, 2585–2600.
7. Zhang, X.; Geng, J.; Xu, Y.; Zhou, Z.; Pang, S. Research on Soft Rocks for the Construction of Roadbeds for High-Speed Railroad: Effect of Water Soaking Environment. *Adv. Mater. Sci. Eng.* **2022**, *2022*, 7070119. [[CrossRef](#)]
8. Yao, Q.; Chen, T.; Tang, C.; Sedighi, M.; Wang, S.; Huang, Q. Influence of moisture on crack propagation in coal and its failure modes. *Eng. Geol.* **2019**, *258*, 105156. [[CrossRef](#)]
9. Chu, F.; Liu, D.; Zhang, X.; Yu, H.; Zhu, G. Dynamic Response and Damage Regularity of Sandstone with Different Moisture States under Cyclic Loading. *Fractal Fract.* **2022**, *6*, 226. [[CrossRef](#)]
10. Li, B.; Yang, F.; Du, P.; Liu, Z. Study on the triaxial unloading creep mechanical properties and creep model of shale in different water content states. *Bull. Eng. Geol. Environ.* **2022**, *81*, 420. [[CrossRef](#)]
11. Hall, K.; Hall, A. Weathering by wetting and drying:some experimental results. *Earth Surf. Process. Landf.* **1996**, *21*, 365–376.
12. Deng, X.; Wang, Y.; Wang, R.; Xia, D.; Zhao, Z. Application of Modified Hoek–Brown Strength Criterion in Water-Rich Soft Rock Tunnel. *Geofluids* **2021**, *2021*, 5552791. [[CrossRef](#)]
13. Turkington, A.V.; Paradise, T.R. Sandstone weathering: A century of research and innovation. *Geomorphology* **2005**, *67*, 229–253. [[CrossRef](#)]
14. Wang, Y.; Liu, Y.; Li, Y.; Jiang, W.; Wang, Y. Experimental Study on the Failure Mechanism of Tunnel Surrounding Rock under Different Groundwater Seepage Paths. *Geofluids* **2021**, *2021*, 8856365. [[CrossRef](#)]
15. Cai, X.; Cheng, C.; Zhao, Y.; Zhou, Z.; Wang, S. The role of water content in rate dependence of tensile strength of a fine-grained sandstone. *Archiv. Civ. Mech. Eng.* **2022**, *22*, 58. [[CrossRef](#)]
16. Lin, H.; Zhang, Q.; Zhang, L.; Duan, K.; Xue, T.; Fan, Q. The Influence of Water Content on the Time-Dependent Mechanical Behavior of Argillaceous Siltstone. *Rock Mech. Rock Eng.* **2022**, *55*, 3939–3957. [[CrossRef](#)]
17. Zhao, K.; Wang, X.; Wang, L.; Zeng, P.; Yang, D.; Jin, J. Investigation of the crack and acoustic emission behavior evolution of red sandstone subjected to water. *Theor. Appl. Fract. Mech.* **2022**, *120*, 103419. [[CrossRef](#)]
18. Huang, X.; Wang, T.; Luo, Y.; Guo, J. Study on the Influence of Water Content on Mechanical Properties and Acoustic Emission Characteristics of Sandstone: Case Study from China Based on a Sandstone from the Nanyang Area. *Sustainability* **2023**, *15*, 552. [[CrossRef](#)]
19. Wei, Z.; Yang, K.; Chi, X.-L.; He, X.; Zhao, X.-Y.; Zhang, J.-Q. Dynamic tensile properties, deformation, and failure testing of impact-loaded coal samples with various water content. *Sci. Rep.* **2021**, *11*, 7096. [[CrossRef](#)]
20. Qin, X.; Zhou, Y.; He, M. Experimental Study on Mechanical Properties and Acoustic Emission Characteristics of Water Bearing Sandstone under Stable Cyclic Loading and Unloading. *Shock. Vib.* **2020**, *2020*, 9472656. [[CrossRef](#)]
21. Li, C.; Liu, N.; Liu, W. Experimental Investigation of Mechanical Behavior of Sandstone with Different Moisture Contents Using the Acoustic Emission Technique. *Adv. Civ. Eng.* **2020**, *2020*, 8877921. [[CrossRef](#)]
22. Zhu, J.; Deng, J.; Chen, F.; Wang, F. Failure analysis of water-bearing rock under direct tension using acoustic emission. *Eng. Geol.* **2022**, *299*, 106541. [[CrossRef](#)]
23. Zhang, Y.; Cao, Y. Mechanical Properties and Failure Mechanism of Granite with Maximum Free Water Absorption under Triaxial Compression. *Appl. Sci.* **2022**, *12*, 3930. [[CrossRef](#)]
24. Yu, Y.; Wang, P.; Zhang, S.; Liu, J. Experimental Study of the Creep Disturbance Effect and Acoustic Emission Characteristics of Mudstone with Different Moisture Contents. *Shock. Vib.* **2021**, *2021*, 7941242. [[CrossRef](#)]
25. You, M.; Hua, A. Fracture of rock specimen and decrement of bearing capacity in uniaxial I compression. *Chin. J. Rock Mech. Eng.* **1998**, *17*, 292–296. (In Chinese)
26. Tarasov, B.; Potvin, Y. Universal criteria for rock brittleness estimation under triaxial compression. *Int. J. Rock Mech. Min. Sci.* **2013**, *59*, 57–69. [[CrossRef](#)]
27. Rickman, R.; Mullen, M.; Petre, E.; Grieser, B.; Kundert, D. *A Practical Use of Shale Petrophysics for Stimulation Design Optimization: All Shale Plays Are Not Clones of the Barnett Shale*; Society of Petroleum Engineers: Denver, CO, USA, 2008.
28. Altindag, R. Assessment of some brittleness indexes in rock-drilling efficiency. *Rock Mech. Rock Eng.* **2010**, *43*, 361–370. [[CrossRef](#)]
29. Liao, D.; Xiao, L.; Zhang, Y. Evaluation model for shale brittleness index based on mineral content and fracture toughness. *Oil Drill. Technol.* **2014**, *42*, 37–41.

30. Cao, Y.; Chen, Y.; Huang, Z. Study on evaluation index of brittleness characteristics of granite under different water content conditions. *J. Eng. Geol.* **2020**, *28*, 29–38. (In Chinese)
31. Zhou, H.; Meng, F.; Zhang, C. Quantitative evaluation of rock brittleness based on stress-strain curve. *Chin. J. Rock Mech. Eng.* **2014**, *33*, 1115–1122. (In Chinese)
32. Aubertin, M.; Gill, D.E.; Simon, R. On the use of the brittleness index modified (BIM) to estimate the post-peak behavior of rock. In Proceedings of the 1st North American Rock Mechanics Symposium, Austin, TX, USA, 1–3 June 1994; pp. 945–952.
33. Jiaqi, G.; Xiliang, L.; Chunsheng, Q. Experimental study of mechanical properties and energy mechanism of karst limestone under natural and saturated states. *Chin. J. Rock Mech. Eng.* **2014**, *33*, 297–307. (In Chinese)
34. Jichen, L.; Linjian, M.; Ning, Z. Research Progress on Energy Evolution in the Process of Rock Deformation and Failure. *Chin. J. Undergr. Space Eng.* **2021**, *17*, 976–986. (In Chinese)

Disclaimer/Publisher's Note: The statements, opinions and data contained in all publications are solely those of the individual author(s) and contributor(s) and not of MDPI and/or the editor(s). MDPI and/or the editor(s) disclaim responsibility for any injury to people or property resulting from any ideas, methods, instructions or products referred to in the content.